Single crystal growth and structural characterization of synthetic U(VI) peroxide phases, studtite ($UO_2(O_2)(H_2O)_2 \cdot 2H_2O$) and metastudtite ($UO_2(O_2)(H_2O)_2$)

Grant C. Benthin[a], Cameron J. Flester[a] , and Tori Z. Forbes*[a]

[a] *Department of Chemistry, University of Iowa, Iowa City, IA 52242, USA*

*Corresponding Authors: Tori Z. Forbes Email: tori-forbes@uiowa.edu

Supporting Information

Contents

1. Studtite Synthesis

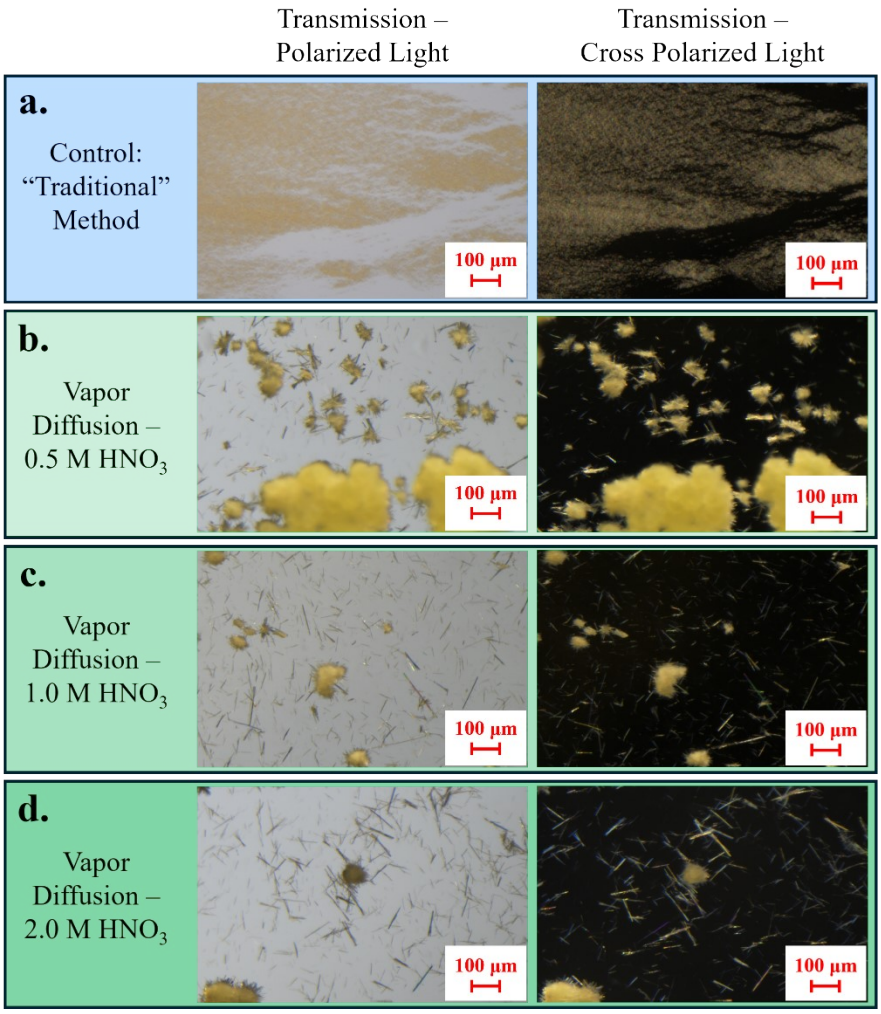

Figure S1. (**a**) Optical microscope images of studtite product grown by direct addition of 30% H_2O_2 into an aqueous uranyl nitrate solution versus (**b-d**) the vapor diffusion of 30% H_2O_2 into uranyl nitrate solutions in varying concentrations of nitric acid. Images were acquired using polarized (left) and cross polarized (right) light in transmission mode.

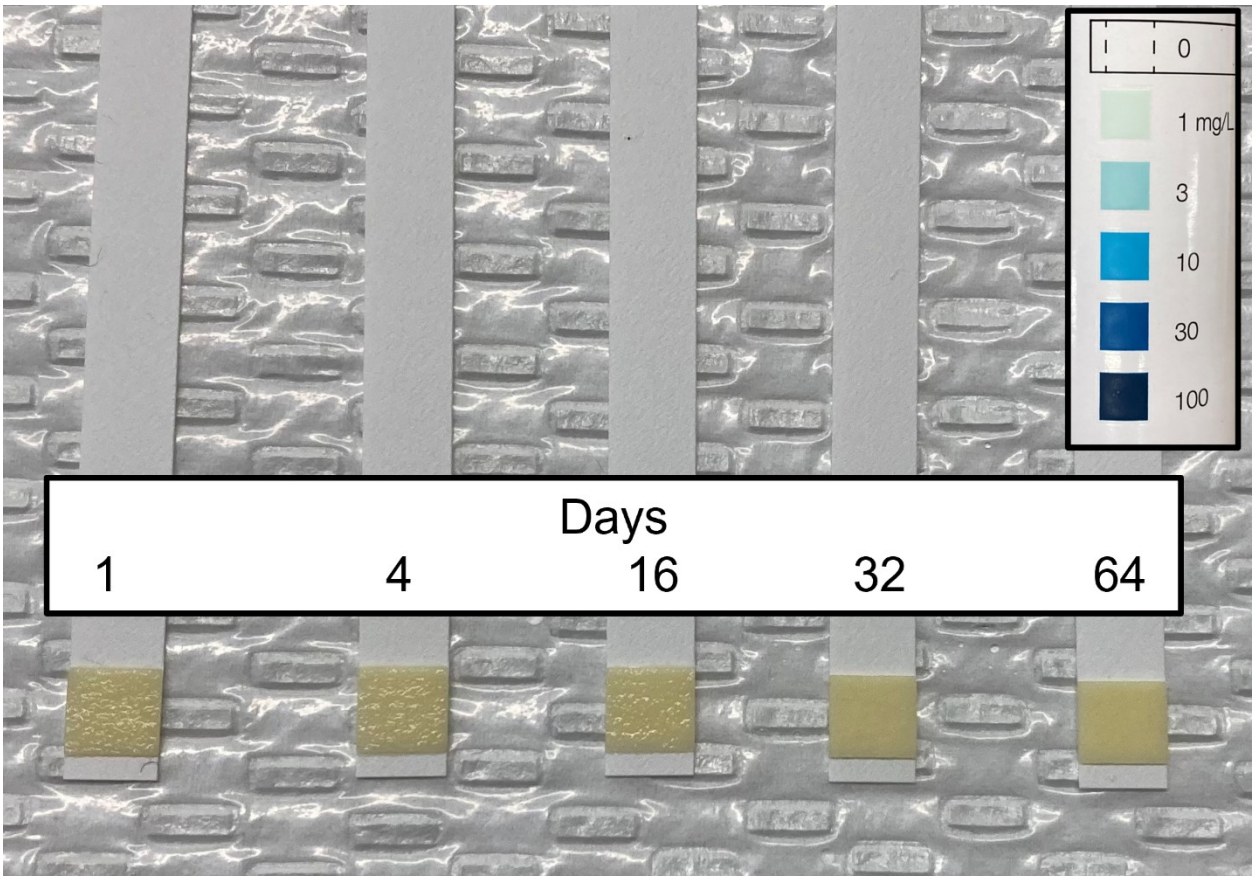

Figure S2. Results of testing peroxide concentration using Qantofix Peroxide 100 test strips in samples of 2 M HNO_3 that were set up for peroxide vapor diffusion for 1, 4, 16, 32, and 64 days. The colors of the test pads indicate that the peroxide concentration is less than 1 mg/L ($3*10^{-5}$ M) for all 5 samples.

2. Dehydration of Studtite to Metastudtite

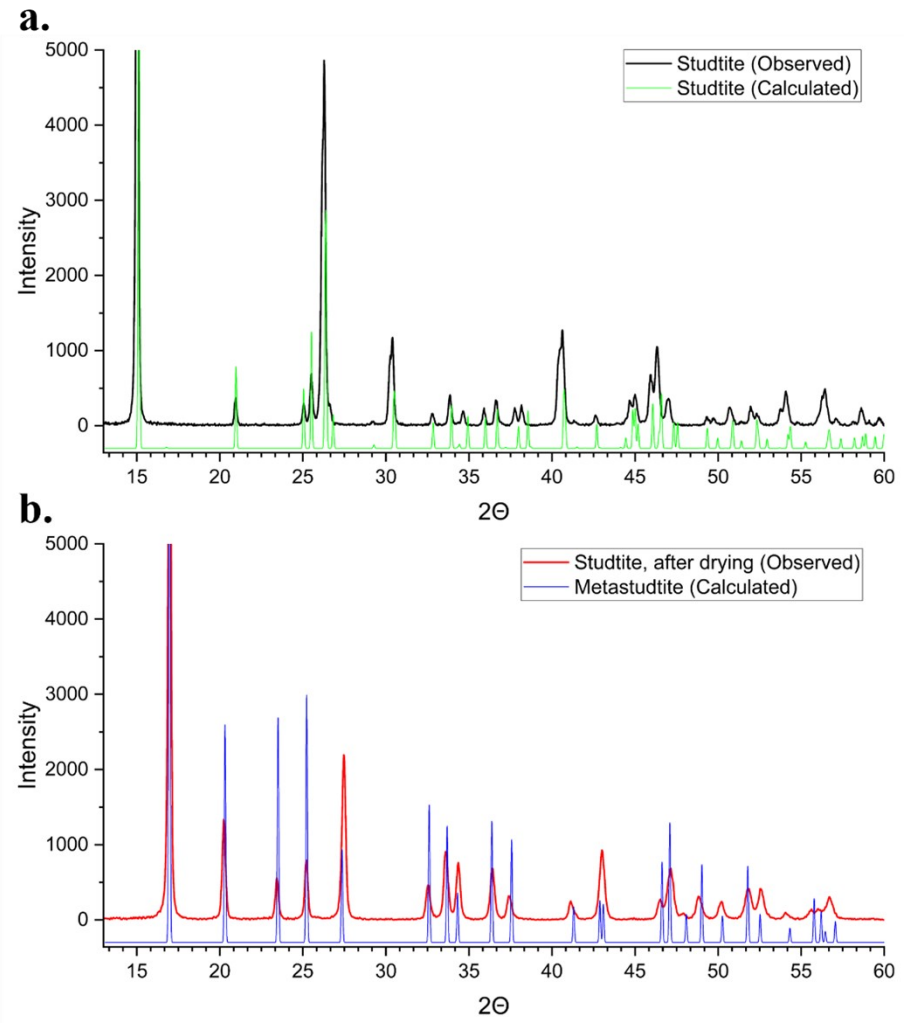

Figure S3. PXRD patterns of (**a**) studtite as synthesized and (**b**) after dehydration in a low humidity environment. Reference patterns of studtite and metastudtite were calculated from the CIF files obtained as a part of the SCXRD analysis in the present work. Data was collected on a Bruker D8 Advance diffractometer (Cu Kα = 1.54 Å) from 10-60 °2θ with a step size of 0.2 °2θ and 1 sec/step.

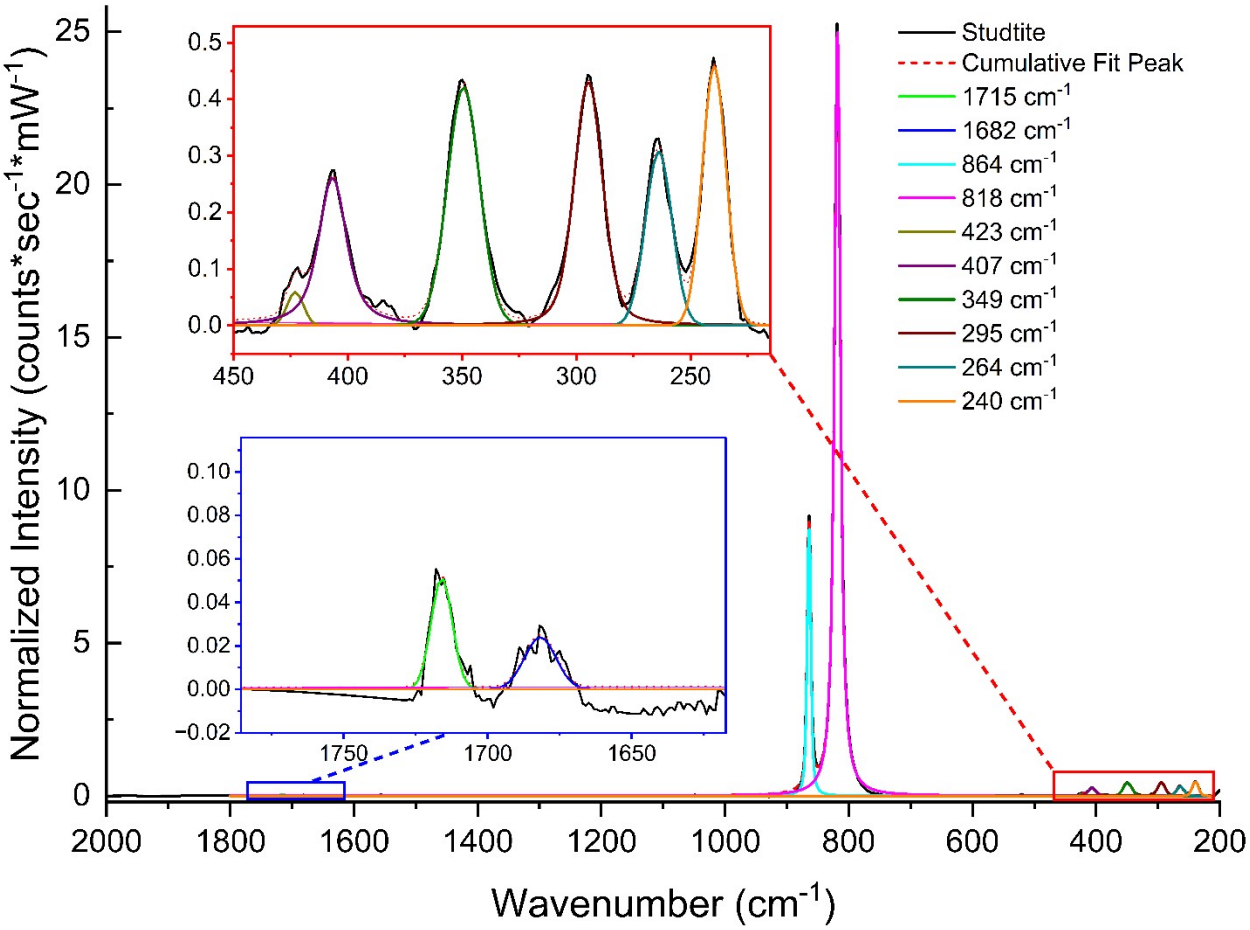

Figure S4. Raman spectra of synthetic crystalline studtite formed through vapor diffusion of hydrogen peroxide. The Raman spectrum was collected (averaged from 3 accumulations) on a Renishaw inVia Raman microscope equipped with a 785 nm laser and a 1200 mm grating with a maximum operating power of 200 mW. The background was subtracted and fit using Origin Pro 9.60 (OriginLab, Northampton, MA).

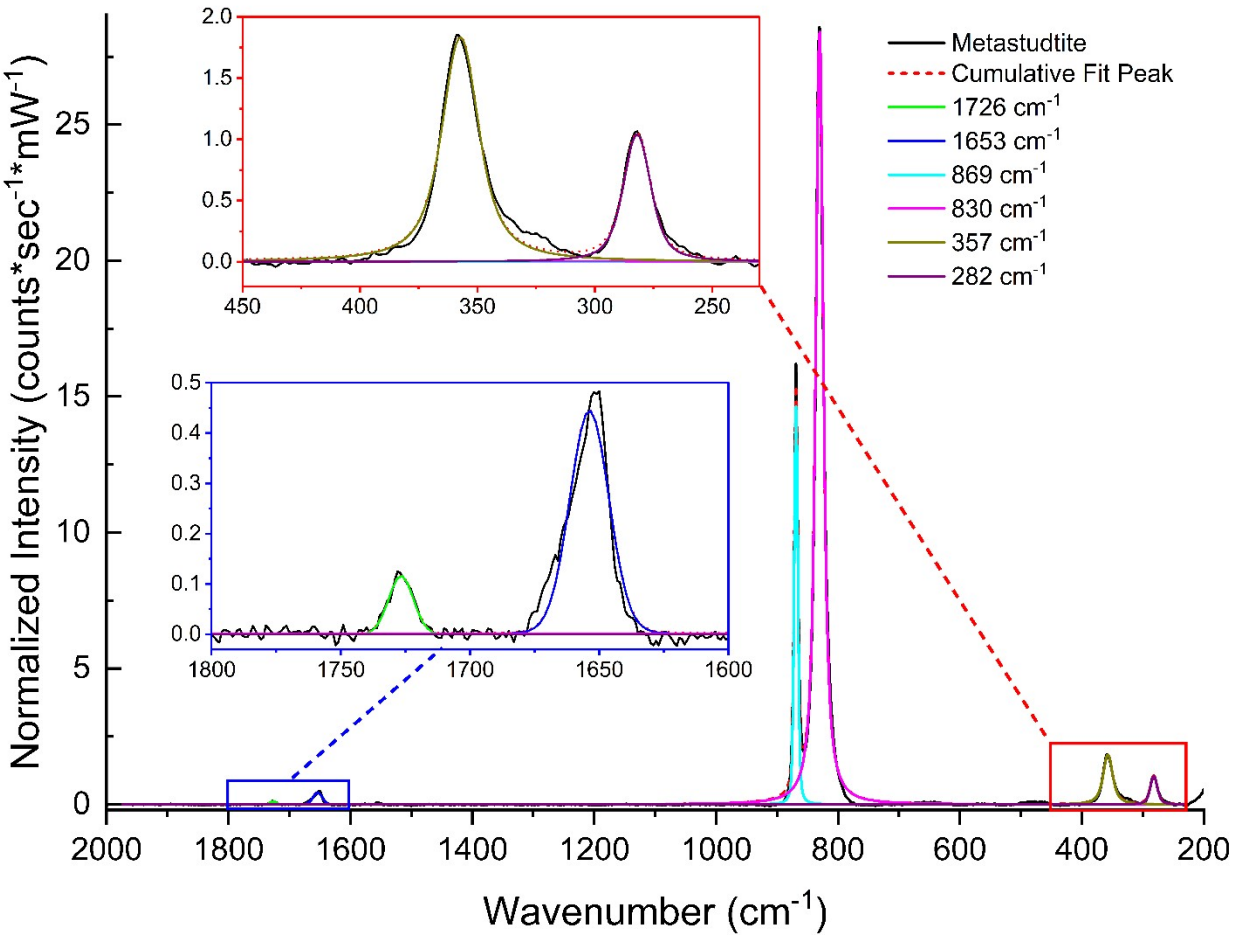

Figure S5. Raman spectra of synthetic metastudtite formed by dehydration of synthetic crystalline studtite in a low humidity environment. The Raman spectrum was collected (averaged from 3 accumulations) on a Renishaw inVia Raman microscope equipped with a 785 nm laser and a 1200 mm grating with a maximum operating power of 200 mW. The background was subtracted and fit using Origin Pro 9.60 (OriginLab, Northampton, MA).

2.1 Interpretation and Discussion of Raman Spectra

The Raman spectra collected on synthetic crystalline studtite before and after exposure to a low relative humidity (<5%) environment for one week (**Fig. S4** and **Fig. S5**) support the conclusion that studtite was dehydrated to form metastudtite. Prior to dehydration, the Raman spectrum of the synthetic studtite shows good agreement with literature reports,[1, 2] with the two most intense features corresponding to the symmetrical stretching modes of the O-O and O=U=O bonds observed at 864 and 818 cm^{-1}, respectively. After one week of exposure to a low relative humidity environment, distinct changes in the Raman spectrum were observed, and the resulting spectrum shows good agreement with literature data for metastudtite.[1] The two most intense features, corresponding to the symmetrical stretching modes of the O-O and O=U=O bonds, are

shifted to 869 and 830 cm^{-1}, respectively. Using the empirical correlation proposed by Bartlett *et al.*,[3] the ν_1 uranyl stretching frequencies were used to estimate U=O bond lengths for both phases. This analysis yielded predicted bond lengths of 1.79(3) Å for studtite and 1.78(3) Å for metastudtite. These values are in good agreement with those obtained from SCXRD (1.795(6) Å and 1.80(2) Å, respectively), providing additional support for the consistency of the spectroscopic and crystallographic results.

3. Single Crystal X-ray Diffraction Analysis

3.1 Analysis of Single Crystals

Crystals of synthetically prepared studtite were isolated from the mother liquor and transferred to a glass slide along with a small amount of Cargille Type NVH immersion oil. Under an optical microscope equipped with rotatable polarized filters, high quality single crystals were isolated and affixed to MiTeGen MicroMounts™ using a minimal amount of Type NVH immersion oil. A suitable crystal was selected and mounted on a Bruker D8 Quest diffractometer equipped with a Mo Kα X-ray source (λ = 0.7107 Å), a PHOTON CMOS integration detector, and an Oxford Cryosystems Cryostream 800 open-flow sample temperature controller. The crystal was kept at 100 K during data collection.

APEX5[4] was used to integrate the data and a multi-scan absorption correction was applied using SADABS-2016/2.[5] wR2(int) was 0.0892 before and 0.0513 after correction. The ratio of minimum to maximum transmission is 0.6537. The λ/2 correction factor is not present. Using Olex2,[6] the structure was solved with the SHELXT structure solution program[7] using intrinsic phasing and refined with the SHELXL refinement package[8] using least squares minimization. O atoms were located and modeled based on the difference Fourier maps. All non-hydrogen atoms were freely refined with anisotropic displacement parameters. The positions of hydrogen atoms were identified from the difference Fourier maps and they were refined with geometric restraints (DFIX and DANG), to allow independent refinement within chemically reasonable limits. For this structure, there is a summary of important crystallographic parameters (**Table S1**), a table of selected bond lengths (**Table S2),** and a depiction of the structure with thermal ellipsoids (**Fig. 1**). The crystallographic information files have been submitted to the CSD and can be found by requesting deposition number 2528711.

For structural characterization of metastudtite, crystals of synthetically prepared studtite were isolated from the mother liquor and transferred to a glass slide along with a small amount of Cargille Type NVH Immersion oil. An optical microscope equipped with rotatable polarized filters was used to identify high quality single crystals which were subsequently isolated and affixed to MiTeGen MicroMounts™ using a minimal amount of Type NVH immersion oil. Crystals were screened on a Bruker D8 Quest diffractometer equipped with a Mo Kα x-ray source (λ = 0.7107 Å), a PHOTON III mixed-mode CPAD detector, and an Oxford Cryosystems Cryostream 700 open-flow sample temperature controller.

Of the approximately 100 crystals that were screened, the 10 best studtite crystals were selected for dehydration. Selection criteria included the correct phase, absence of twinning, and the highest degree of crystallinity. These crystals (still affixed to mounts) were placed in small jars (300 cm^3) containing calcium sulfate desiccant for one week. After dehydration, a suitable crystal was selected and placed back on the diffractometer used for the initial screening. The crystal was kept at 100 K during data collection.

APEX5[4] was used to integrate the data and a multi-scan absorption correction was applied using SADABS-2016/2.[5] The λ/2 correction factor is not present. Using Olex2,[6] the structure was solved with the SHELXT structure solution program[7] using intrinsic phasing and refined with the SHELXL refinement package[8] using least squares minimization. Atoms O2 and O3 were located and modeled with ½ occupancy based on the difference Fourier maps. All non-hydrogen atoms were freely refined with anisotropic displacement parameters. The positions of hydrogen atoms were identified from the difference Fourier maps and they were refined with geometric restraints (DFIX and DANG), to allow independent refinement within chemically reasonable limits. We note that the CIFCheck suggests a Z = 4 but the actual structure contains Z= 2. For this structure, there is a summary of important crystallographic parameters (**Table S1**), a table of selected bond lengths (**Table S3**), and a depiction of the structure with thermal ellipsoids (**Fig. 2**). The crystallographic information files have been submitted to the ICSD and can be found by requesting deposition number 2528712.

3.2 Evaluation of Alternative Metastudtite Structural Models

The presence of apparent disorder within the uranyl–peroxide chains prompted us to evaluate alternative structural models involving symmetry reduction and supercell expansion. These models were created to assess whether the observed disorder could be resolved by adopting a lower-symmetry space group.

First, the crystallographic model proposed by Weck *et al.* for metastudtite, which adopts an orthorhombic space group *Pnma* (Z = 4) with lattice parameters a ≈ 8.45 Å, b ≈ 8.72 Å, and c ≈ 6.75 Å, was evaluated as a starting point.[9] However, application of this unit cell and symmetry to the present diffraction data did not yield a stable refinement. In particular, refinement attempts resulted in poorly behaved displacement parameters and did not eliminate the apparent disorder associated with the peroxide and uranyl oxygen positions. These observations indicate that the ordered *Pnma* model is not consistent with the present dataset.

To further assess the possibility of resolving the disorder by decreasing symmetry a series of alternative space groups derived from or related to the parent orthorhombic lattice were tested using the experimentally determined unit cell. These included orthorhombic subgroups (e.g., *Pmmm*, *Pnnm*, *Pmmn*) as well as lower-symmetry and subgroup-related settings (e.g., *I*2/*m*, *I*222, I2*mm*). In these models, symmetry constraints on the oxygen positions are reduced, allowing splitting of sites and potential ordering of the uranyl–peroxide chains. However, refinement of these alternative models did not lead to meaningful improvements in R-factors or residual electron density. In many cases, refinements of these alternative models were unstable or resulted in chemically unreasonable geometries, including distorted uranium coordination geometries and displacement parameters that were unrealistically large, highly anisotropic, or non-positive definite. Importantly, none of these models resolved the apparent disorder.

Given that the repeat unit of the uranyl–peroxide chains is approximately 8.4 Å, roughly twice the length of the a-axis in the refined *Immm* model, a supercell was also evaluated by doubling the

a-axis to allow for possible long-range ordering of peroxide and uranyl orientations. Despite this increased structural freedom, refinement of the supercell model did not resolve the disorder, and no evidence for long-range ordering of the peroxide groups and uranyl oxygens was observed.

Overall, these results strongly suggest that the observed disorder is not an artifact of the imposed crystallographic symmetry or limited unit cell dimensions. Instead, the persistence of disorder across all tested models suggests that it is an intrinsic feature of the uranyl–peroxide chain arrangement.

4. Crystallographic Information Table and Figures

Table S1. Selected crystallographic information of synthetic studtite and metastudtite

Compound	**Natural studtite (Burns *et al.*[10])**	**Studtite**	**Metastudtite**
Structural Fromula	$[(UO_2)O_2(H_2O)_2]\cdot 2H_2O$	$[(UO_2)O_2(H_2O)_2]\cdot 2H_2O$	$(UO_2)O_2(H_2O)_2$
Crystal color and habit	-	Light Yellow, Needle	Light Yellow, Needle
Formula weight (g)	374.09	374.09	338.06
Space group	Monoclinic, *C2/c*	Monoclinic,*C2/c*	Orthorhombic, *Immm*
a (Å)	14.068(6)	13.999(1)	4.1946(5)
b (Å)	6.721(3)	6.7481(7)	6.5143(9)
c (Å)	8.428(4)	8.4848(9)	8.733(1)
α (°)	90	90	90
β (°)	123.356(6)	123.143(3)	90
γ (°)	90	90	90
Unit cell volume ($Å^3$)	665.7(3)	671.1(1)	238.65(6)
Density, ρ (g/cm^3)	3.73	3.702	4.704
Z	4	4	2
μ (mm^{-1})	24.4	24.180	33.938
F(000)	656	656.0	288.0
Θ range (°)	3 to 69	6.952 to 50.772	7.804 to 50.832
Limiting indices	$-100 \le h \le 100$, $-100 \le k \le 100$, $-100 \le l \le 100$	$-16 \le h \le 16$, $-8 \le k \le 8$, $-10 \le l \le 9$	$-5 \le h \le 5$, $-7 \le k \le 7$, $-10 \le l \le 10$
Ref. collected/unique	6416/1398	3119/619	3334/143
R_{int}	-	0.0403	0.0617
Data/restraints/parameters	-	619/6/60	143/2/23
GOF on F^2	-	1.226	1.198
R_1 ([I>2σ(I)])	-	0.0281	0.0350
wR_2 ([I>2σ(I)])	-	0.0427	0.0843
R_1 (all data)	0.0366	0.0493	0.0350
wR_2 (all data)	0.0760	0.0478	0.0843
Largest diff. peak/hole (e $Å^{-3}$)	-	0.80/-0.90	3.48/-0.66
CCDC deposition number	1656578	2528711	2528712

Table S2. Bond distance table for natural studtite vs. synthetic studtite.

	Natural Studtite (Burns *et al.*[10])			Synthetic Studtite (Present Work)		
Bond Type	**Atom1**	**Atom2**	**Length (Å)**	**Atom1**	**Atom2**	**Length (Å)**
$U\text{-}O_{\text{-yl}}$	U1	O1	1.768(7)	U1	O1	1.795(6)
$U\text{-}O_{peroxo}$	U1	O2	2.351(6)	U1	O2	2.373(6)
	U1	O2	2.364(6)	U1	O2	2.380(6)
$U\text{-}O_{aqua}$	U1	O3	2.396(7)	U1	O3	2.417(6)
$O_{peroxo}\text{-}O_{peroxo}$	O2	O2	1.46(1)	O2	O2	1.50(1)
$O_{aqua}\text{-}H$	O3	H1	0.98	O3	H3A	0.97(2)
	O3	H2	0.97	O3	H3B	0.97(2)
$O_{water}\text{-}H$	O4	H3	0.97	O4	H4A	0.96(2)
	O4	H4	0.97	O4	H4B	0.96(2)

Table S3. Bond distance table for the experimentally determined metastudtite structure vs. the computationally derived metastudtite structure.

	Experimental Metastudtite (Present Work)			Computationally Derived Metastudtite (Weck *et al.*[9])		
Bond Type	**Atom1**	**Atom2**	**Length (Å)**	**Atom1**	**Atom2**	**Length (Å)**
$U\text{-}O_{\text{-yl}}$	U1	O1	1.80(2)	U1	O1	1.851
	-	-	-	U1	O2	1.803
$U\text{-}O_{peroxo}$	U1	O2	2.35(1)	U1	O3	2.388
	-	-	-	U1	O3	2.387
$U\text{-}O_{aqua}$	U1	O3	2.42(2)	U1	O4	2.422
$O_{peroxo}\text{-}O_{peroxo}$	O2	O2	1.47(4)	O3	O3	1.455
$O_{aqua}\text{-}H$	O3	H3	0.97(2)	O4	H1	0.999
	-	-	-	O4	H2	0.990

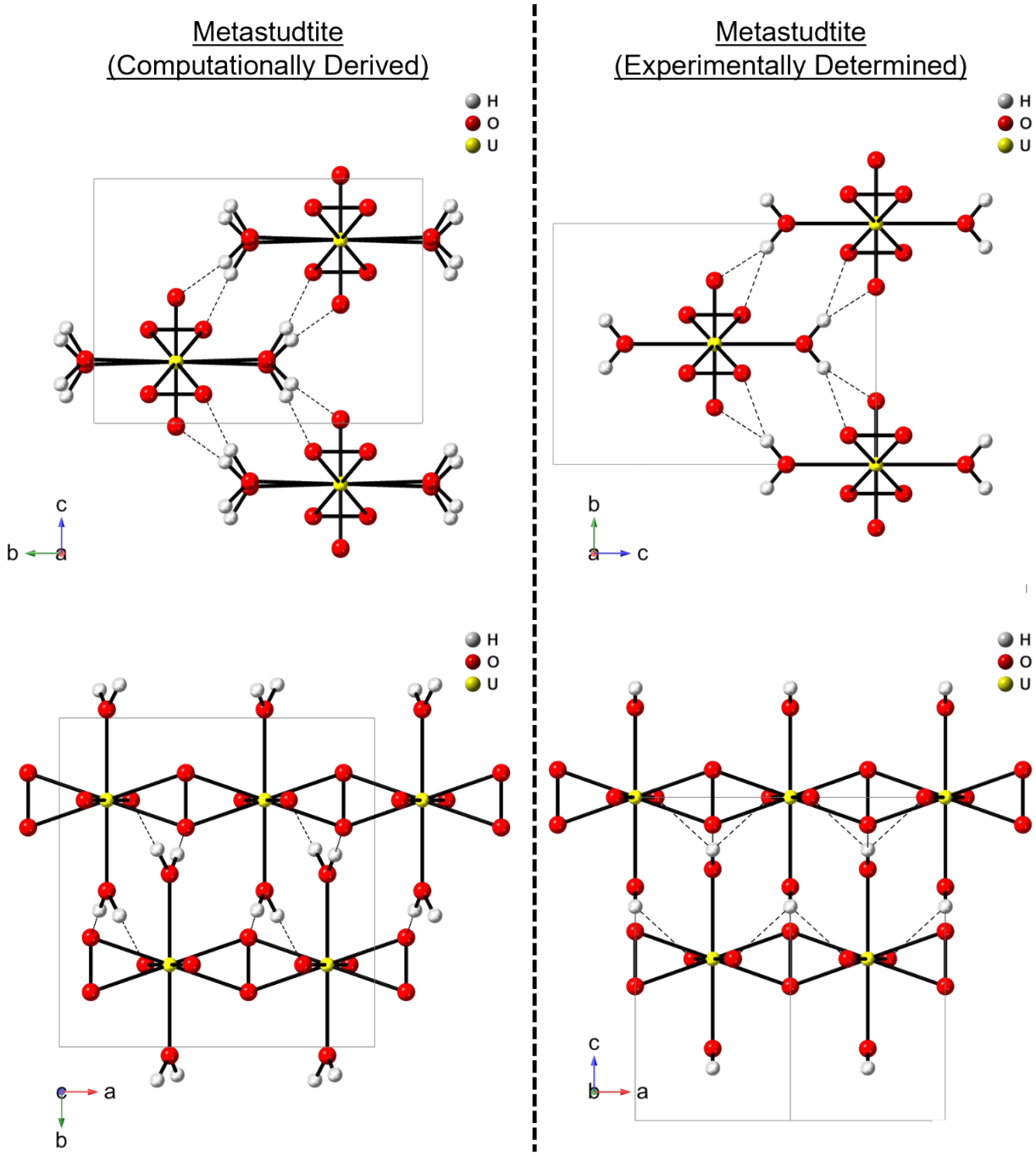

Figure S6. Ball and stick models of the computationally derived metastudtite structure[9] (left) compared to the experimentally determined metastudtite structure (right). For clarity, only ½ of the disorder in the chains of the experimental structures is shown.

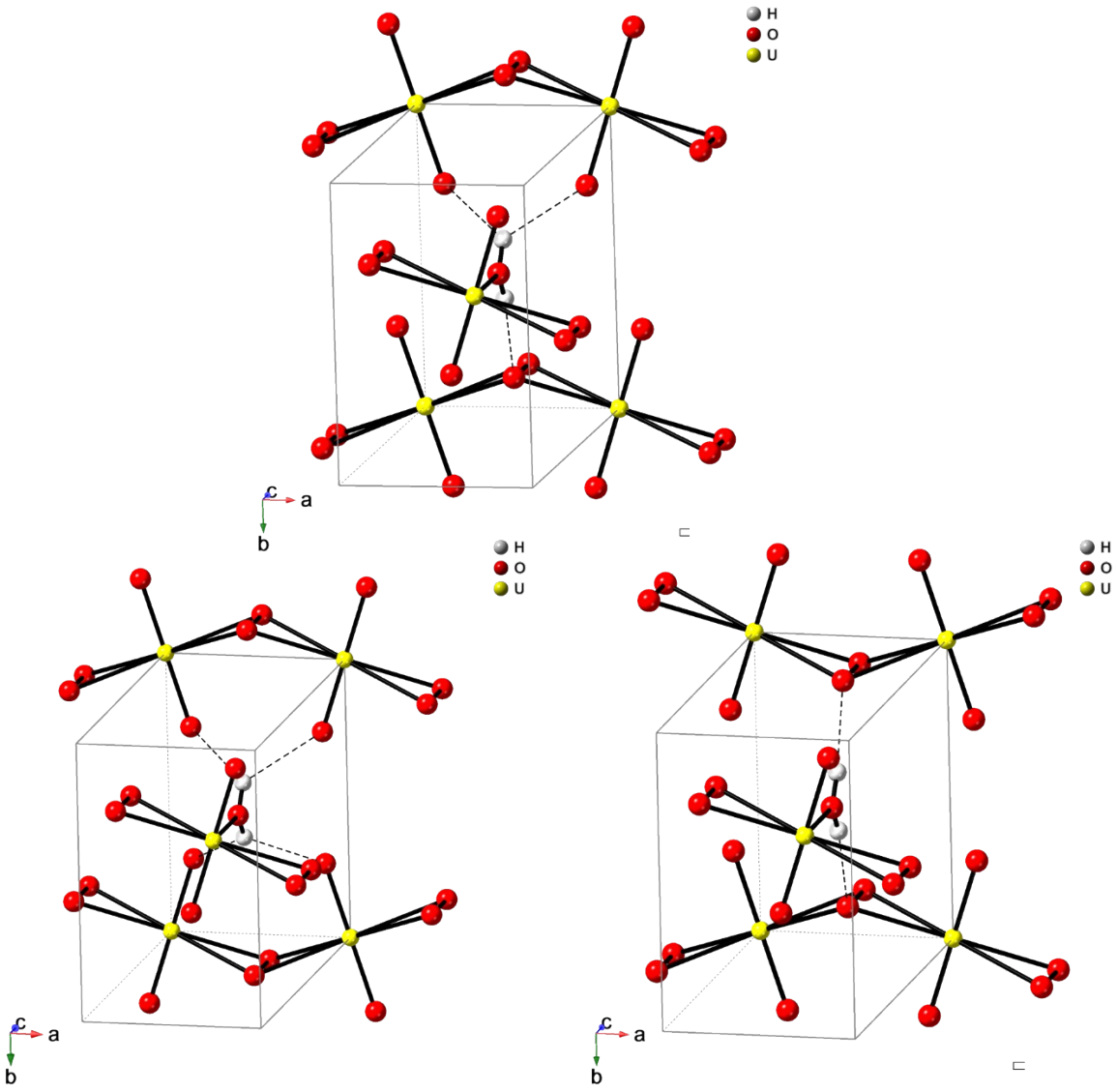

Figure S7. The different possible configurations of adjacent metastudtite chains. With the peroxo bridges oriented in the same direction, each equatorial aqua ligand participates in 3 hydrogen bonding interactions (two with oxo ligands and one with a peroxo ligand). With the chains oriented in opposite directions, each equatorial aqua ligand participates in either 4 hydrogen bonding interactions (all four with oxo ligands) or two bonding interactions (both with peroxo ligands).

References

(1) Bastians, S.; Crump, G.; Griffith, W. P.; Withnall, R. Raspite and studtite: Raman spectra of two unique minerals. *Journal of Raman Spectroscopy* **2004**, *35* (8-9), 726-731. DOI: https://doi.org/10.1002/jrs.1176.
(2) Colmenero, F.; Bonales, L. J.; Cobos, J.; Timón, V. Study of the thermal stability of studtite by in situ Raman spectroscopy and DFT calculations. *Spectrochimica Acta Part A: Molecular and Biomolecular Spectroscopy* **2017**, *174*, 245-253. DOI: https://doi.org/10.1016/j.saa.2016.11.040.
(3) Bartlett, J. R.; Cooney, R. P. On the determination of uranium□oxygen bond lengths in dioxouranium(VI) compounds by Raman spectroscopy. *Journal of Molecular Structure* **1989**, *193*, 295-300. DOI: https://doi.org/10.1016/0022-2860(89)80140-1.
(4) *APEX5*; Bruker AXS Inc: Madison, Wisconsin, USA, 2023. (accessed 2023).
(5) *SADABS-2016/2*; Bruker AXS Inc: (accessed 2023).
(6) Dolomanov, O. V.; Bourhis, L. J.; Gildea, R. J.; Howard, J. A. K.; Puschmann, H. OLEX2: a complete structure solution, refinement and analysis program. *Journal of Applied Crystallography* **2009**, *42* (2), 339-341. DOI: doi:10.1107/S0021889808042726.
(7) Sheldrick, G. SHELXT - Integrated space-group and crystal-structure determination. *Acta Crystallographica Section A* **2015**, *71* (1), 3-8. DOI: doi:10.1107/S2053273314026370.
(8) Sheldrick, G. M. A short history of SHELX. *Acta Crystallographica Section A* **2008**, *64* (1), 112-122. DOI: doi:10.1107/S0108767307043930.
(9) Weck, P. F.; Kim, E.; Jové-Colón, C. F.; Sassani, D. C. Structures of uranyl peroxide hydrates: a first-principles study of studtite and metastudtite. *Dalton Transactions* **2012**, *41* (32), 9748-9752, 10.1039/C2DT31242E. DOI: 10.1039/C2DT31242E.
(10) Burns, P. C.; Hughes, K.-A. Studtite, [(UO2)(O2)(H2O)2](H2O)2: The first structure of a peroxide mineral. *American Mineralogist* **2003**, *88* (7), 1165-1168. DOI: 10.2138/am-2003-0725 (acccessed 7/16/2024).